Switching-based Adaptive Active Control for Periodic Noises in Unknown 3D Environment

Chengxi Zhong, Qilong Zhang, Guanqi He, Song Liu *Member, IEEE*, and Yang Wang *Member, IEEE*

***Abstract*— Active noise control (ANC) or active disturbance rejection techniques have been extensively explored to mitigate unwanted noise/disturbance across diverse applications. Existing mainstream approaches typically employ filter-based feedforward or feedback methods. However, there still lacks the capability of asymptotically and completely canceling multi-harmonic noises. In this paper, we introduce a novel switching-based adaptive controller to handle this problem, supporting a complete cancellation of unmeasurable multi-sinusoidal noises featuring arbitrary frequencies from unmodeled three-dimensional (3D) environments, without the concern of waterbed effect. The proposed controller utilizes an online adaptive law to estimate the frequency response at the relevant frequencies based solely on information from the error microphone. Notably, the overall dimension of the controller remains relatively low, regardless of the number of noise frequencies. Experimental results highlight the unprecedented adaptive multi-sinusoidal noise cancellation performance with an average reduction of more than -30 dB in terms of amplitude. The asymptotic stability proof is also given in the paper.**

I. Introduction

The active control of noises or disturbances [1] has achieved great success in modern robotics [2], industrial processes [3], and automation systems [4]. As a promising technique, active noise control (ANC) aims to mitigate unwanted noises by virtue of generating anti-noise sound waves that destructively interfere with coming-forth unwanted sound noises [5]. Despite the accomplishments so far, there still exist limitations when addressing extensive 3D spaces [6], [7], particularly in intricate and unfamiliar systems characterized by unknown 3D environments perturbed by an unmeasurable periodic noise source spanning multiple low frequencies, such as vehicle interior and construction site [8]–[10]. Additionally, the pivotal requisites of global convergence and noise reduction performance remain unsolved [11]. Thus, a critical demand arises for an effective ANC strategy that can achieve complete cancellation of periodic noises featuring arbitrary multiple-harmonic frequencies in an unknown 3D space with global asymptotic stability.

*This work was in part supported by the National Natural Science Foundation of China under Grant 62303321. (Chengxi Zhong and Qilong Zhang contribute equally to this work.) (*Corresponding author: Song Liu and Yang Wang*.)

C. Zhong, and Q. Zhang are with the School of Information Science and Technology, ShanghaiTech University, Shanghai 201210, China (email: zhongchx, zhangql1@shanghaitech.edu.cn)

G. He is with the Robotics Institute, Carnegie Mellon University, Pittsburgh, PA, USA (e-mail: guanqihe@andrew.cmu.edu)

S. Liu and Y. Wang are with the School of Information Science and Technology, ShanghaiTech University, Shanghai 201210, China, and with Shanghai Engineering Research Center of Intelligent Vision and Imaging, Shanghai, China (e-mail: liusong, wangyang4@shanghaitech.edu.cn)

State-of-the-art (SOTA) filter-based ANC approaches fall into feedforward-based methods [7] or feedback-based ones [12]. For feedforward-based, the least-mean-square-based filter [13] and its derivatives [14]–[16] are representative. For instance, FxLMS [17] dynamically adjusts the coefficients of a control filter to generate anti-noise waves that attenuate the primary noise at a specified location. Its straightforward and understandable structure makes it easy to implement. However, filter-based feedforward methods exhibit certain weaknesses, e.g., the limited cancellation ability and the potential instability brought by the acoustic coupling between the primary path and the secondary path [18]. Therefore, it is imperative to have prior knowledge or online identification of the critical transfer function of the secondary path [19]. Furthermore, the feedforward methods essentially require a reference microphone mounted near the source noise (see Fig. 1).

On the contrary, filter-based feedback ANC methods function without the reference microphone. This allows them to circumvent the instability problem that can arise due to inaccuracies in estimating the secondary path. Furthermore, the efficacy of noise reduction in this system hinges solely on the active loudspeaker, adaptive controller, and error microphones, resulting in a notably reduced implementation cost (Fig. 1). Nevertheless, it is essential to acknowledge its inherent limitations. Primarily, stability concerns still exist, similar to the infinite impulse response (IIR) filter [20]. Another weakness is the 'waterbed effect' [21], which implies that whenever noise reduction is achieved at specific frequencies within a feedback ANC system, an increase in noise levels can be expected at other frequencies. Therefore, these drawbacks necessitate careful consideration and modulation for specific applications, which makes the ANC across all frequencies in an unknown 3D space practically unattainable. Moreover, the above-discussed techniques cannot achieve complete cancellation of periodic noise at specific frequencies with limited attenuation of around -10 to -20 dB [22].

In this work, we introduce a novel switching-based adaptive controller for complete cancellation of multi-sinusoidal noises from unmodeled 3D space with asymptotic stability. Its adaptability allows for the precise alignment of noise sources at arbitrary locations, without system modeling and the information of the surrounding environment, enhancing its resilience against unexpected shifts in source noise and error microphone. The rest of this paper is organized as follows: Section II states the addressed problem; Section III presents the design and asymptotic stability of the proposed controller; Section IV gives detailed experimental results.

Manuscript 518 submitted to 2024 IEEE International Conference on Robotics and Automation (ICRA). Received September 10, 2023.

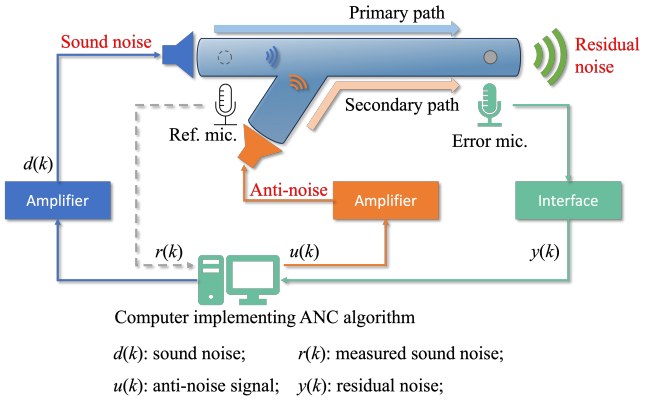

Fig. 1: Standard ANC system setup with and without reference microphone. The feedforward-based ANC approach necessitate reference microphone, while the feedback-based ANC approach works only on error microphone.

II. Problem Statement

A. Standard ANC System

Fig. 1 conceptually depicts the fundamental elements of standard ANC system, manifesting two distinct pathways: the *Primary Path* and the *Secondary Path*. The *Primary Path* encompasses the route between the noise loudspeaker and the error microphone, while the *Secondary Path* refers to the path between the anti-noise loudspeaker and the error microphone. In this work, the feedback structure without a reference microphone is considered. In specific:

- The **Noise loudspeaker** serves as an artificial noise generator and has the ability to reproduce various types of sound noise with distinct characteristics.
- The **Anti-noise loudspeaker**, functioning as an actuator, delivers the anti-noise signal to the system based on algorithmic calculations.
- The **Error microphone** is strategically positioned at the open end of the system. Its main purpose is to collect the residual noise, providing necessary information for active noise control.
- The **Computing platform** is responsible for generating noise signals, receiving information collected by microphones, and generating anti-noise signals based on various ANC algorithms.

B. Mathematical Description of ANC System

In contrast to the conventional ANC algorithm, which typically models the primary path and secondary path separately [18], we adopt an approach where the ANC setup in Section II-A is regarded as a discrete linear time-invariant (LTI) single-input single-output (SISO) system. The mathematical representation can be expressed as follows:

$$\begin{aligned} x(k+1) &= Ax(k) + B\big[u(k) + d(k)\big] \\ y(k) &= Cx(k) \end{aligned} \tag{1}$$

where $x(k)$ denotes the *unmeasurable* state variables, $d(k)$ represents the *unmeasurable* sound noise, $u(k)$ signifies the anti-noise signal, and $y(k)$ is regarded as the residual noise, picked up by the error microphone. The propagation of sound in the unknown 3D environment is modeled by the matrices A, B, and C. However, explicit knowledge regarding the structure of A, B, and C is not required.

Our primary objective is to devise an anti-noise signal $u(k)$ that effectively minimizes the undesirable sound noise $d(k)$ solely based on the information provided by the residual noise $y(k)$, without relying on detailed knowledge of the system model (1), i.e. matrices A, B, and C. Furthermore, the sound noise $d(k)$ examined in this paper follows a specific pattern, as expressed by the following assumption:

Assumption 1: The sound noise $d(k)$ is formed by the combination of N distinct sinusoidal signals:

$$d(k) = \sum_{n=1}^{N} \psi_n \sin(\omega_n k + \phi_n), \tag{2}$$

each sinusoidal signal is characterized by a **known** frequency $\omega_n > 0$, but the amplitude and phase ($\psi_n > 0$, $\phi_n \in (-\pi, \pi]$) are **unknown**. These individual signals are aggregated to form the overall sound noise $d(k)$. ◁

It is worth mentioning that, by the nature of the ANC problem, the state variables of system (1) exhibit bounded behavior over time when subjected to bounded inputs or disturbances, without requiring external stabilization mechanisms. Hence, in accordance with the standard assumption for the output regulation problem [23], we have that system (1) is internally stable.

III. Switching-based Adaptive Active Noise Controller

A. Controller Design

The fundamental idea of our controller is to estimate the sound noise $d(k)$ and generate a signal $u(k)$ opposite to $d(k)$ in order to achieve complete noise elimination. Our controller aims to require as little system information as possible and maintain a relatively low dimension (linearly increases with the number of noise frequencies). To achieve these goals, we follow our preliminary work [24] and propose a novel discrete-time switching-based adaptive active noise controller in this paper, which takes on the following specific form:

$$\begin{aligned} u(k) &= \Gamma \hat{v}(k) \\ \hat{v}(k+1) &= S\hat{v}(k) - \varepsilon G \hat{\boldsymbol{\theta}}_{\sigma}^{\top}(k) \hat{\zeta}_o(k) \\ \hat{\zeta}_o(k+1) &= F_{\varepsilon}(k)\hat{\zeta}_o(k) - \alpha \Gamma^{\top}\big[\Gamma \hat{\zeta}_o(k) - y(k)\big] \end{aligned} \tag{3}$$

where $\hat{v}(k) \in \mathbb{R}^{2N}$ is utilized to generate an estimate of the sound noise $d(k)$. As there is an estimation process, there is bound to be estimation error. However, since the sound noise itself is not directly measurable, obtaining the estimation error is typically not possible. To overcome this challenge, we introduce an observer denoted as $\hat{\zeta}_o(k) \in \mathbb{R}^{2N}$, which is employed to correct the estimation error and drive it towards zero.

Manuscript 518 submitted to 2024 IEEE International Conference on Robotics and Automation (ICRA). Received September 10, 2023.

$\hat{\boldsymbol{\theta}}_\sigma(k)$ and $F_\varepsilon(k)$ in (3) will be explained later in (10), while S, G, and Γ are constant matrices defined as follows:

$$S = \mathrm{diag}(S_1, \ldots, S_N),\ S_n = \begin{bmatrix} \cos\omega_n & \sin\omega_n \\ -\sin\omega_n & \cos\omega_n \end{bmatrix},$$
$$g = [1, 0]^\top,\ G = \mathrm{diag}(g, \ldots, g),\ \Gamma = [g^\top, \ldots, g^\top], \tag{4}$$

where $\mathrm{diag}(\cdot)$ denotes the diagonal matrix operation. The parameters ε and α correspond to positive gains, and it is important to choose both of them to be sufficiently small.

*1) **Adaptive Law**:* According to the internal model principle [25], to completely cancel out the sound noise $d(k)$, it is imperative to gain information about the frequency response of system (1) at each frequency ω_n, where $n \in \mathcal{N} = \{1, 2, \ldots, N\}$, which is defined by:

$$\theta_n^\top(\omega_n) := \left[\mathrm{Re}\big(H(e^{j\omega_n})\big) \quad -\mathrm{Im}\big(H(e^{j\omega_n})\big)\right], \tag{5}$$

where $H(e^{j\omega_n}) = C(e^{j\omega_n} \cdot I - A)^{-1}B$, $\mathrm{Re}(\cdot)$ and $\mathrm{Im}(\cdot)$ denote the real and imaginary parts, respectively. Despite the essentiality of $\theta_n(\omega_n)$, given the 3D environment unknown, obtaining accurate values of $\theta_n(\omega_n)$ beforehand is impossible. To address this issue, we introduce an online adaptive law to estimate the frequency response $\theta_n(\omega_n)$ at each frequency ω_n. The adaptive law utilizes the error between the expected canceling effect and the currently achieved canceling effect, which can be represented by:

$$\eta_n(k+1) = \eta_n(k) - \gamma\hat{\xi}_{1,n}(k)\big[\Gamma\hat{\zeta}_o(k) - y(k) - \textstyle\sum_{n=1}^{N}\tilde{\theta}_n^\top(k)\hat{\xi}_{1,n}(k)\big], \tag{6}$$

where $\eta_n(k)$ denotes the estimate of the frequency response $\theta_n(\omega_n)$ at each frequency ω_n, γ is a positive tuning gain, $\tilde{\theta}_n(k)$ will be defined later, and $\hat{\xi}_{1,n}(k)$ represents the $(2n-1)$-th and $2n$-th elements of the regressor signal $\hat{\xi}_1(k)$. The update equation for $\hat{\xi}_1(k+1)$ is given by:

$$\hat{\xi}_1(k+1) = F_\alpha^\top\hat{\xi}_1(k) - \varepsilon G\hat{\boldsymbol{\theta}}_\sigma^\top(k)\hat{\zeta}_o(k), \tag{7}$$

where $F_\alpha = S - \alpha\Gamma^\top\Gamma$ is a stable constant matrix.

*2) **Switching Mechanism**:* During the ANC process, $\eta_n(k)$ is a fast-updated signal, which may lead to instability issues if directly implemented in the controller. Therefore, to ensure the stability of the closed-loop system, we devise a novel switching mechanism to replace $\eta_n(k)$ with a surrogate signal $\hat{\theta}_{\sigma_n(k)}$. First, we select M different points within the 2D plane as constant candidate estimates for each frequency response $\theta_n(\omega_n)$, denoted as $\hat{\theta}_m^\top = [\hat{\theta}_{m,1}, \hat{\theta}_{m,2}]$, where $m \in \mathcal{M} := \{1, 2, \ldots, M\}$. Next, at each time step k, we calculate the distance between the fast-updated estimate $\eta_n(k)$ and the constant estimate $\hat{\theta}_m$ as the monitoring signal $\pi_n^m(k)$:

$$\pi_n^m(k) = \|\eta_n(k) - \hat{\theta}_m\|,\ n \in \mathcal{N},\ m \in \mathcal{M}. \tag{8}$$

Then, for each frequency ω_n, we select the candidate estimate $\hat{\theta}_m$ that is closest to $\eta_n(k)$ as the surrogate signal $\hat{\theta}_{\sigma_n(k)}$ and combine them to form $\hat{\boldsymbol{\theta}}_\sigma(k)$. Finally, we consider a rare and pathological scenario where $\eta_n(k)$ may be equidistant from multiple candidate estimates, potentially resulting in infinite fast switching. To prevent this case, we further propose a hysteresis modification on the switching logic $\sigma_n(k)$, which can be expressed as follows:

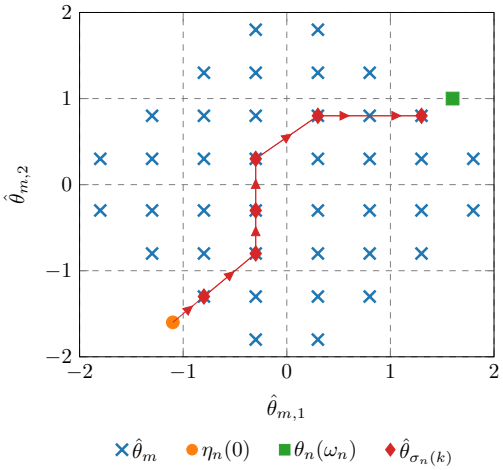

Fig. 2: The schematic diagram of the switching mechanism.

$$\sigma_n(k) = \underset{\sigma_n(k^-),m}{\arg\min}\{\pi_n^m, \pi_n^{\sigma_n(k^-)} - h\}, \tag{9}$$

where $m \in \mathcal{M}\backslash\{\sigma_n(k^-)\}$, $\sigma_n(k^-)$ indicates the index of the candidate estimate selected at the previous time step, and h is a small positive parameter used to avoid infinite fast switching. The hysteresis logic demonstrates that if $\eta_n(k)$ has the minimum distance to multiple candidate estimates, we still maintain the candidate estimate selected previously.

Hence, the aforementioned $\hat{\boldsymbol{\theta}}_\sigma(k)$ and $F_\varepsilon(k)$ at time step k are formed as follows:

$$\hat{\boldsymbol{\theta}}_\sigma(k) = \mathrm{diag}(\hat{\theta}_{\sigma_1(k)}, \ldots, \hat{\theta}_{\sigma_N(k)})$$
$$F_\varepsilon(k) = S - \varepsilon\hat{\boldsymbol{\theta}}_\sigma(k)\hat{\boldsymbol{\theta}}_\sigma^\top(k) \tag{10}$$

Additionally, the term $\tilde{\theta}_n(k) = \hat{\theta}_{\sigma_n(k)} - \eta_n(k)$ in (6) stands for the error signal between $\hat{\theta}_{\sigma_n(k)}$ and $\eta_n(k)$.

The initial conditions for the controller are set to zero, except for $\eta_n(0)$, which is initialized at a predetermined location. $\hat{\theta}_m$ that serve as candidate frequency response estimates are selected to be uniformly distributed across the entire 2D plane.

Fig. 2 provides a brief illustration of the proposed switching mechanism. Initially, the nearest $\hat{\theta}_m$ to $\eta_n(0)$ is selected as the initial $\hat{\theta}_{\sigma_n(0)}$. As $\eta_n(k)$ gradually approaches the frequency response $\theta_n(\omega_n)$ through the adaptive law (6), correspondingly, $\hat{\theta}_{\sigma_n(k)}$ driven by the switching mechanism (9) will also switch to the candidate estimate $\hat{\theta}_m$ that is closest to $\theta_n(\omega_n)$.

B. Asymptotic Stability Analysis

In this part, we aim to theoretically demonstrate the effective cancellation of the noise $d(k)$ via a brief analysis of the system (1) along with the adaptive controller (3).

First, we need to formulate the energy function, commonly referred to as the Lyapunov function, in order to prove the asymptotic stability of the closed-loop system which

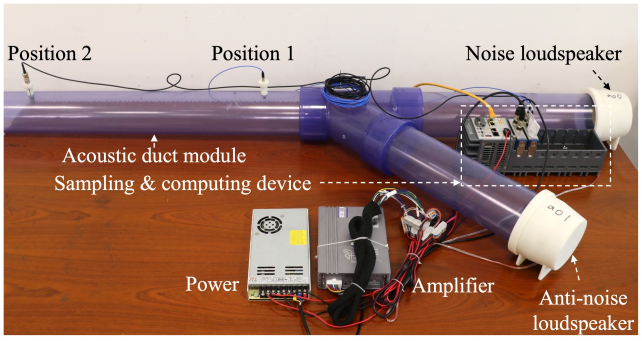

Fig. 3: The prototyped ANC system setup.

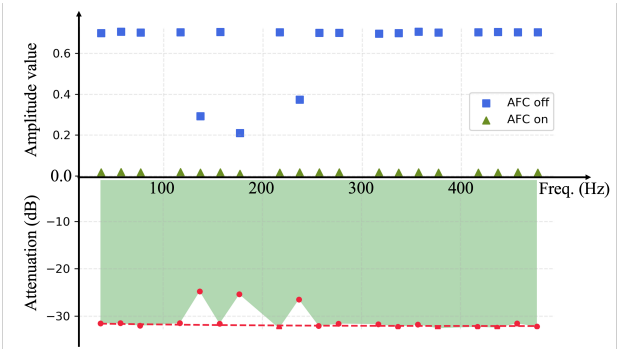

Fig. 4: Noise attenuation performance over frequency spectrum.

indicates the success of the complete cancellation of the noise. Let us denote the energy function as follows:

$$V(\hat{\zeta}_o, \hat{\xi}_1, x, \tilde{\theta}_n) = V_1(\hat{\zeta}_o) + V_2(\hat{\xi}_1) + V_3(x) + V_4(\tilde{\theta}_n) \quad (11)$$

with $V_1(\hat{\zeta}_o) = \hat{\zeta}_o^\top(k) P_\varepsilon \hat{\zeta}_o(k)$, $V_2(\hat{\xi}_1) = \hat{\xi}_1^\top(k) P_\alpha \hat{\xi}_1(k)$, $V_3(x) = x^\top(k) P_x x(k)$, and $V_4(\tilde{\theta}_n) = 1/2\tilde{\theta}_n^\top(k)\theta_n(k)$. Here, P_ε, P_α, and P_x are all positive-definite matrices that fulfill the criteria of Lyapunov equations for matrices F_ε, $F_\alpha^\top$, and A, respectively. The fundamental logic behind demonstrating the effectiveness of our controller lies in analyzing the difference $\Delta V(k)$ along the trajectories of the closed-loop system. By appropriately choosing the parameters ε, α, γ, and h, we can establish the condition $\Delta V(k) < 0$, indicating that the energy function $V(\hat{\zeta}_o, \hat{\xi}_1, x, \tilde{\theta}_n)$ decreases as time progresses towards infinity. Consequently, all components contained in $y(k)$ converge towards zero, ultimately leading to the convergence of the residual noise $y(k)$ to zero as well. Due to constraints on available space, we regretfully omit the comprehensive explanations. For a similar derivation, we kindly invite readers to refer to the detailed analysis procedure outlined in [23].

The provable theoretical result is summarized as follows:

Theorem 1: Assuming that Assumption 1 is satisfied, it can be inferred that the ANC system defined by equation (1), guided by the switching-based adaptive controller described in equation (3), and the corresponding switching-based adaptive law given by equations (6) and (9), possesses the capability to effectively mitigate the sound noise $d(k)$ as represented in equation (2), provided that the adjustable parameter gains ε, α, γ, and h are appropriately selected. ◁

IV. Experiments and Results

To comprehensively evaluate the proposed controller, we carried out experiments from three aspects including single frequency noise cancellation, composite frequency noise cancellation, and the SOTA comparison. The details are provided in the forthcoming subsections.

A. System Setup and Implementation Details

As shown in Fig. 3, we have key components including a noise loudspeaker, an anti-noise loudspeaker, two microphones, a power source, an amplifier, sampling unit, and computing device. We've designed an acoustic duct module with two separate paths for handling noise and anti-noise signals. In the primary path, the noise loudspeaker generates simulated noise, while the anti-noise loudspeaker produces an anti-noise signal in the secondary path. The computing device is based on a cRIO-9049 NI 8-channel controller with a 1.60 GHz quad-core CPU, 4 GB DRAM, and 16 GB storage, suitable for real-time control systems. Sampling unit is done using an NI 9250 sound acquisition card with 2 channels and a synchronous sampling rate of 102.4 kS/s, to capture residual noise from the strategically placed error microphones. By transmitting the anti-noise signal optimized by controller via the secondary path, we achieve constructive interference at the target position, effectively canceling out noise from the primary path. The acoustic module is equipped with multiple error microphone positions, which can create different 3D environments by changing the microphone's placement. For the proposed controller, we set parameters ε, α, γ, and h to 0.01, 0.01, 0.02, and 0.1, while γ is adjusted to 0.005 for composite noise cancellation evaluation. The sampling time is set as 0.002 s.

B. Single Frequency Noise Cancellation

*1) **Noise Attenuation Efficacy**:* Firstly, for introduced noise signals featured with distinct single frequency, we measured their amplitudes (represented as royal blue squares) and corresponding residual noise signals after applying our controller (represented as olive green triangles), whose results are shown in Fig. 4. The substantial amplitude reduction indicated our controller's effectiveness in attenuating noise signals with individual frequencies. Based on a quantitative metric of decibel (dB) attenuation given as

$$\text{Attenuation (dB)} = 20 \times \log_{10}\left(\frac{\text{Amp}_{after}}{\text{Amp}_{before}}\right), \quad (12)$$

an average attenuation of -30.95 dB was achieved. Notably, there were three kinds of frequencies (137, 177, and 237 Hz) representing different levels of noise before attenuation, whereby we observed a consistent amplitude of residual noise after attenuation. It highlighted our controller's ability to effectively reduce noise amplitudes to a stable level, regardless of the initial noise amplitude.

Then, we explored the convergence behavior in the time domain for single frequency noise. From Fig. 5 (a), we found

Manuscript 518 submitted to 2024 IEEE International Conference on Robotics and Automation (ICRA). Received September 10, 2023.

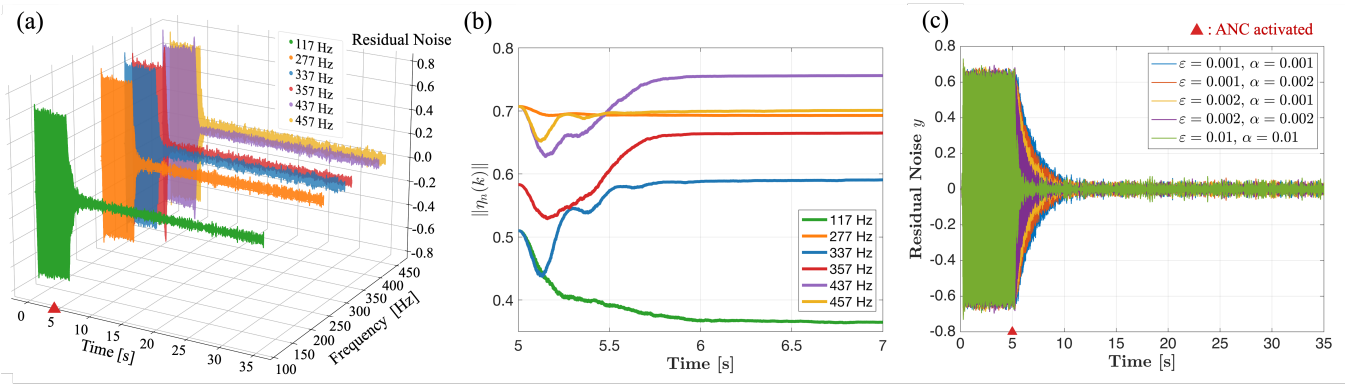

Fig. 5: Single frequency noise cancellation performance in terms of (a) time domain noise attenuation efficacy (b) convergence of the adaptive parameters, and (c) hyper-parameter effects.

that the significant noise reduction for each single frequency was achieved as soon as the controller activated at 5 seconds. Moreover, the convergence rates across different frequencies were remarkably uniform, indicating a consistency of our controller in reducing residual noise with a single frequency.

*2) **Convergence of the Adaptive Parameters**:* We visualized the trajectory of the norm of the adaptive signal, i.e. the estimate $\eta_n(k)$ of the frequency response of the system (1) over different frequencies. As illustrated in Fig. 5 (b), for different frequencies of interest, $\eta_n(k)$ all converged to a constant value within 1 second, demonstrating adaptability of our controller to arbitrary unknown 3D environment and indicating that the remaining residual noise in Fig. 5 (a) is not primarily caused by algorithm convergence issues but rather by measurement errors stemming from the limitations of microphone performance.

*3) **Hyper-Parameters Effects**:* Furthermore, we varied key hyper-parameters i.e., ε controlling the optimization step size and α determining the weight assigned to the regularization term, over a predefined range. In Fig. 5 (c), the amplitude evolution of the residual noise y illustrated the hyper-parameters effects on the controller's noise cancellation performance. It was observed that variations in ε and α affected the convergence speed, where larger ε and higher α expedited the convergence process, leading to faster noise reduction. Despite the influence of the convergence rate, they didn't compromise the final noise suppression significantly, highlighting the robustness of our controller in terms of varied hyper-parameter settings.

*4) **Adaptability to Distinct 3D Environment**:* Different error microphone positions represent entirely different environments. Despite this variability, our controller demonstrated a remarkable generality to distinct systems. By relocating the microphone from position 1 to position 2 in Fig. 3, a few single frequency noise cancellation experiment has been re-conducted and the performance are summarized in Table I. Remarkably, the achieved suppression effects remained consistent after this repositioning. Thus, our controller is independent of the specific error microphone arrangement, demonstrating its robust adaptability within the unknown 3D environment.

TABLE I: The attenuation performance for position 2 system

Freq. (Hz)	Before Att	After Att	Att (dB)
37	0.6995	0.0178	-31.8874
137	0.7000	0.0173	-32.1410
237	0.6986	0.0179	-31.8275
337	0.7000	0.0183	-31.6529
437	0.6987	0.0185	-31.5424

C. Composite Frequency Noise Cancellation

*1) **Noise Attenuation Efficacy**:* We conducted experiments focused on composite frequency noise featuring five distinct frequencies including 67, 167, 267, 367, and 467 Hz. Fig. 6 (a) illustrated the pre- and post-effectiveness of the proposed controller when dealing with composite frequencies. Even in scenarios involving composite frequencies, our controller was capable of achieving effective noise attenuation in a short amount of time and consistently maintaining the same level of attenuation with the single frequency case, i.e. around -31 dB.

*2) **Sequence of Switching Signals** $\hat{\theta}_{\sigma_n(k)}$:* To illustrate the novel switching mechanism described by equation (9), we provided the switching process of the signal $\hat{\theta}_{\sigma_n(k)}$ for partial frequency components (167, 267, and 367 Hz) in Fig. 6 (b). Due to the unknown 3D environment, the actual position of the frequency response $\theta_n(\omega_n)$ cannot be obtained, so only $\eta_n(k)$ at the final moment 25 second can be plotted. Fig. 6 (b) showed that $\hat{\theta}_{\sigma_n(k)}$ selected and switched to $\hat{\theta}_m$ closest to $\eta_n(k)$, and as $\eta_n(k)$ approached the real frequency response $\theta_n(\omega_n)$, $\hat{\theta}_{\sigma_n(k)}$ also kept switching to $\hat{\theta}_m$ closest to the real frequency response.

*3) **SOTA Comparison**:* Finally, we conducted further quantitative comparison among our controller, FxLMS [26], and MAML [22] when dealing with composite frequencies noise. During comparison, the control filter and the secondary path estimate have 64 and 32 steps with a step size of 0.0002 and a sampling rate of 5 kHz. As shown in Fig. 6 (c), the extension of each radar line in each frequency direction represented the attenuation (dB) formulated as Eq. (12), while the area indicated the composite noise cancel-

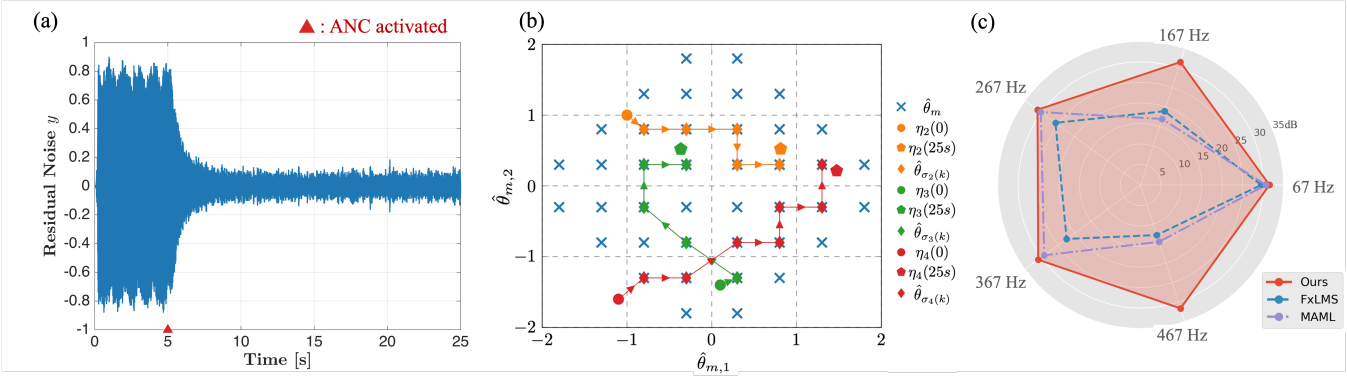

Fig. 6: Composite frequency noise cancellation performance in terms of (a) time domain noise attenuation efficacy, (b) sequence of switching signals, and (c) SOTA comparison.

lation capability in all frequencies. FxLMS demonstrated better noise reduction capabilities in low-frequency scenarios while MAML, benefiting from pre-trained filter coefficient initial values, achieved comparable suppression effects to our proposed controller, however, falling short of providing comprehensive coverage across the entire frequency spectrum. On the contrary, our controller exhibited consistent extension lengths across each frequency direction and a substantial area for composite frequencies, depicting an average composite noise attenuation of approximately -31 dB.

More quantitative comparison results are given in Table II, which indicates that the proposed controller ensured an average attenuation of approximately -31.3828 dB with an attenuation variance of about 0.0743 across distinct frequencies. It also demonstrated a quick convergence which is approximately 18,961 steps (3.7922 seconds). In summary, these findings underscored the controller's effectiveness, versatility, and consistent performance in addressing complex composite noise scenarios and its superior noise cancellation capability and stability with a comparable convergence speed compared to SOTA methods [26] [22].

TABLE II: SOTA comparison in terms of attenuation, consistency, and convergence speed

Method	Avg. Att (dB)	Var. Att	Convg. Time
FxLMS	-21.8904	41.1297	4.9088
MAML	-24.3112	62.0915	**2.6756**
Ours	**-31.3828**	**0.0743**	3.7922

D. Discussion

ANC is a critical area of research and engineering, particularly in the implementation of robotic and automation systems. Mechanical vibrations induced by motor actuation, as well as noise in industrial scenarios, often manifest as periodic disturbances, which can lead to unexpected mechanical failures and operational challenges. While our approach was initially designed and tested within the context of active sound noise control, it is important to recognize its versatility and potential applicability in diverse domains. The fundamental concept of actively suppressing disturbances through the generation of counteracting signals similar to our proposed controller for ANC can be explored further for potential extensions. For instance, it can aid in reducing the impact of external forces or perturbations on the robot's trajectory to enhance its overall performance and suppressing vibrations caused by motor movements in robot arms to ensure more accurate and stable manipulation of objects. It also can be employed to suppress vibrations in machinery, thereby prolonging equipment lifespan and reducing maintenance costs. In conclusion, by actively controlling noises or disturbances, one can enhance the performance, efficiency, and safety of various systems, paving the way for widespread adoption of this valuable technology.

V. Conclusions

This study presents an innovative switching-based adaptive controller designed to achieve comprehensive multi-sinusoidal noise elimination within an unmodelled 3D space, while ensuring global asymptotic stability and convergency. The inherent adaptability of this controller facilitates the accurate alignment of noise sources situated at arbitrary locations, all without necessitating complex system modeling or detailed knowledge of the ambient surroundings. This intrinsic flexibility not only enhances the controller's efficacy but also bolsters its ability to withstand unforeseen variations in noise source locations and errors in microphone placement. By introducing a solution that transcends the limitations of conventional approaches, this work contributes to the advancement of noise cancellation techniques, holding great promise for practical applications in real-world scenarios. In future work, we will investigate the controller's performance in more complex and dynamic environments as well as integrate it with machine learning techniques.

References

[1] P. A. Nelson and S. J. Elliott, *Active control of sound*. Academic Press, 1991.

[2] J. Borenstein and Y. Koren, "Noise rejection for ultrasonic sensors in mobile robot applications," in *Proc. IEEE Int. Conf. Robot. Autom.*, 1992, pp. 1727–1732.

[3] J. Furusho, G. Zhang, and M. Sakaguchi, "Vibration suppression control of robot arms using a homogeneous-type electrorheological fluid," in *Proc. IEEE Int. Conf. Robot. Autom.*, vol. 4, 1997, pp. 3441–3448.

[4] L. Ott, F. Nageotte, P. Zanne, and M. de Mathelin, "Physiological motion rejection in flexible endoscopy using visual servoing and repetitive control : Improvements on non-periodic reference tracking and non-periodic disturbance rejection," in *Proc. IEEE Int. Conf. Robot. Autom.*, 2009, pp. 4233–4238.

[5] S. M. Kuo and D. R. Morgan, *Active noise control systems: algorithms and DSP Implementations*. New York: Wiley, 1996.

[6] M. Kamaldar and J. B. Hoagg, "Adaptive harmonic control for rejection of sinusoidal disturbances acting on an unknown system," *IEEE Trans. Control Syst. Technol.*, vol. 28, no. 2, pp. 277–290, 2018.

[7] D. Shi, W.-S. Gan, B. Lam, and S. Wen, "Feedforward selective fixed-filter active noise control: Algorithm and implementation," *IEEE/ACM Trans. Audio Speech Lang. Process.*, vol. 28, pp. 1479–1492, 2020.

[8] S. Wang, H. Li, P. Zhang, J. Tao, H. Zou, and X. Qiu, "An experimental study on the upper limit frequency of global active noise control in car cabins," *Mech. Syst. Signal Process.*, vol. 201, p. 110672, 2023.

[9] S. Kim and M. E. Altinsoy, "A complementary effect in active control of powertrain and road noise in the vehicle interior," *IEEE Access*, vol. 10, pp. 27 121–27 135, 2022.

[10] N. Kwon, M. Park, H.-S. Lee, J. Ahn, and M. Shin, "Construction noise management using active noise control techniques," *J. Constr. Eng. Manag.*, vol. 142, no. 7, p. 04016014, 2016.

[11] G. Chen and K. Muto, "A theoretical study of convergence characteristics of a multiple channel anc system," *Int. J. Acoust. Vib.*, vol. 9, no. 4, pp. 191–197, 2004.

[12] M. Tufail, S. Ahmed, M. Rehan, and M. T. Akhtar, "A two adaptive filters-based method for reducing effects of acoustic feedback in single-channel feedforward anc systems," *Digit. Signal Process.*, vol. 90, pp. 18–27, 2019.

[13] S. D. Stearns, *Of aldapfive signal processing*, 1985.

[14] J. Lorente, M. Ferrer, M. de Diego, and A. Gonzalez, "The frequency partitioned block modified filtered-x nlms with orthogonal correction factors for multichannel active noise control," *Digit. Signal Process.*, vol. 43, pp. 47–58, 2015.

[15] O. J. Tobias and R. Seara, "Leaky-fxlms algorithm: Stochastic analysis for gaussian data and secondary path modeling error," *IEEE Trans. Speech Audio Process.*, vol. 13, no. 6, pp. 1217–1230, 2005.

[16] D. Shi, W.-S. Gan, B. Lam, and C. Shi, "Two-gradient direction fxlms: An adaptive active noise control algorithm with output constraint," *Mech. Syst. Signal Process.*, vol. 116, pp. 651–667, 2019.

[17] S. M. Kuo and D. R. Morgan, "Active noise control: a tutorial review," *Proc. IEEE*, vol. 87, no. 6, pp. 943–973, 1999.

[18] T.-B. Airimitoaie, I. D. Landau, R. Melendez, and L. Dugard, "Algorithms for adaptive feedforward noise attenuation—a unified approach and experimental evaluation," *IEEE Trans. Control Syst. Technol.*, vol. 29, no. 5, pp. 1850–1862, 2020.

[19] C.-Y. Chang, S. M. Kuo, and C.-W. Huang, "Secondary path modeling for narrowband active noise control systems," *Appl. Acoust.*, vol. 131, pp. 154–164, 2018.

[20] T. Saramäki, *Finite impulse reponse filter design*. John Wiley & Sons, 1993, pp. 155–277.

[21] L. Wu, X. Qiu, and Y. Guo, "A generalized leaky fxlms algorithm for tuning the waterbed effect of feedback active noise control systems," *Mech. Syst. Signal Process.*, vol. 106, pp. 13–23, 2018.

[22] D. Shi, W.-S. Gan, B. Lam, and K. Ooi, "Fast adaptive active noise control based on modified model-agnostic meta-learning algorithm," *IEEE Signal Process. Lett.*, vol. 28, pp. 593–597, 2021.

[23] Y. Wang, G. Pin, A. Serrani, and T. Parisini, "Removing spr-like conditions in adaptive feedforward control of uncertain systems," *IEEE Trans. Autom. Control*, vol. 65, no. 6, pp. 2309–2324, 2020.

[24] G. He, Y. Wang, G. Pin, A. Serrani, and T. Parisini, "Switching-based adaptive output regulation for uncertain systems affected by a periodic disturbance," in *Proc. Amer. Control Conf. (ACC)*, 2022.

[25] M. Bin, D. Astolfi, and L. Marconi, "About robustness of control systems embedding an internal model," *IEEE Trans. Autom. Control*, vol. 68, no. 3, pp. 1306–1320, 2023.

[26] D. R. Morgan, "History, applications, and subsequent development of the fxlms algorithm [dsp history]," *IEEE Signal Process. Mag.*, vol. 30, no. 3, pp. 172–176, 2013.